

Co-delivery of chitosan nanoparticles of 5-aminolevulinic acid and shGBAS for improving photodynamic therapy efficacy in oral squamous cell carcinomas

Xing Wang^{a,b,1}, Shufang Li^{a,1}, Hongwei Liu^{a,*}

^a Department of Oral Medicine, Peking University School and Hospital of Stomatology, Beijing, China

^b Department of Stomatology, Chinese PLA General Hospital, Beijing, China

ARTICLE INFO

Keywords:

shGBAS
Oral squamous cell carcinoma
Chitosan
Photodynamic therapy
Mitochondria

ABSTRACT

Background: The improvement of gene therapy provides hope for the treatment of cancer. However, malignant tumor is a multifactorial disease, which remains difficult to be cured with a single therapy. Our previous study reported that mitochondrial genes glioblastoma-amplified sequence (GBAS) plays a role in the development and treatment of oral squamous cell carcinoma (OSCC). The current study focused on building a mitochondrial-targeting drug co-delivery system for combined photodynamic therapy (PDT) and gene therapy.

Methods: 5-aminolevulinic acid (ALA) photosensitizer loaded chitosan (CS) nanoparticles were prepared using ionic crosslinking method, and further synthesized with the GBAS gene plasmid DNA (shGBAS) by electrostatic attraction. We detected the effects of PDT using the co-delivery system (CS-ALA-shGBAS) on cell proliferation and mitochondrial injury by MTT and reactive oxygen species (ROS) assays, respectively. Additionally, a oral cancer Xenograft model of nude mice was built to test its inhibitive effect on the cancerous growth *in vivo*.

Results: A novel nanocomposite, CS-ALA-shGBAS, was found to be spherical structures and had good dispersion, stability and hypotoxicity. Gel retardation assay showed that CS-ALA nanoparticle could synthesize shGBAS at and above Nanoparticle/Plasmid ratios of 1/2. Excitingly, the co-delivery system was suitable for transfected cells and displayed a superior mitochondrially targeted killing effect on OSCC *in vitro* and *in vivo*.

Conclusion: Our study provides evidence that the chitosan-based co-delivery system of ALA-induced protoporphyrin IX (PpIX) photosensitizer and GBAS gene may be a novel mode of combined therapy for OSCC.

1. Introduction

Oral cancer is one of the most frequent malignancies in the head and neck region, with squamous cell carcinoma being by far the most common pathology type, accounting for 90 % [1]. Despite two decades of advances in cancer therapy, it is less treatable with existing remedies because of multi-factorial risk factors. Based on the data of Chinese National Cancer Center, the overall mortality rate of oral cancer is as high as 1.26/100,000 in the world's most populous nation [2]. Multi-disciplinary therapy regimen has become the principal part in the treatment of the medium and advanced oral squamous cell carcinoma (OSCC), including operation, radio-chemical therapy, biotherapy and others. In addition to therapeutic effect benefits, researchers have been

trying to seek the minimally invasive topical treatment option and lead better quality of life in advanced OSCC patients [3,4].

Photodynamic therapy (PDT) is a relatively new and developing modality for the treatment of oral cancer and precancer [5]. Light, photosensitizer, and oxygen are the three elements of photodynamic effect. Numerous studies have revealed that PDT not only has direct inhibition function on tumor cells but also induce specific antitumor immune response. Our previous studies found that 5-aminolevulinic acid-mediated PDT (ALA-PDT) can eliminate the oral precancerous lesions and diminish the normal tissue damage under the local anesthesia [6,7]. A recent review found evidence that PDT is effective for oral cancers as either a primary or alternative intervention [8]. PDT can generate large amounts of oxygen-rich molecules of the type known as

* Corresponding author at: Department of Oral Medicine, Peking University School and Hospital of Stomatology, 22 Zhongguancun South Avenue, Haidian District, Beijing, China.

E-mail address: hongwei12569@163.com (H. Liu).

¹ These authors contributed equally to this work.

<https://doi.org/10.1016/j.pdpdt.2021.102218>

Received 15 January 2021; Received in revised form 2 February 2021; Accepted 8 February 2021

Available online 13 February 2021

1572-1000/© 2021 Elsevier B.V. All rights reserved.

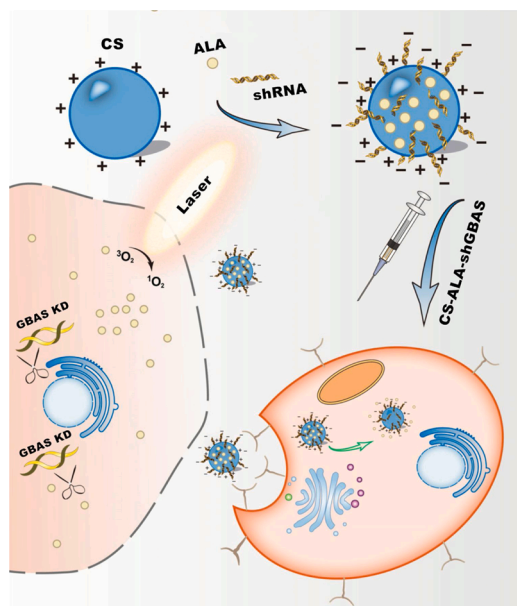


Fig. 1. Schematic illustration of the co-delivery chitosan nanoparticles of ALA and shGBAS for improving PDT in cancer cells.

reactive oxygen species (ROS) in cancer cells, in turn affecting the biological behaviour of tumor.

ALA is one of the most widely used photosensitizers in oncologic therapeutic areas, whose fast development has greatly raised the level of clinical diagnosis and treatment. ALA is the naturally occurring precursor of protoporphyrin IX (PpIX), indirectly lead to photosensitization when irradiated with a specific wavelengths of light [9]. The subcellular localization of photosensitizers may be the most important influence factor of PDT. Broadly speaking, ALA-PDT can not only suppress the inner mitochondrial membrane enzymes production, but also decrease the mitochondrial membrane potential [10,11]. Our previous research also demonstrated that ALA-PDT could induce mitochondrial photooxidative stress, leading to obvious changes in expression of MMPs, and inhibiting the growth of oral cancer cells [7]. However, the PDT resistance remains a main barrier to the long-term maintenance of its effect on oral cancer cells [12]. This fact designates the further direction of PDT regimens for OSCC treatment, mainly those in which mitochondria targeting drugs may improve the anti-tumor effect of PDT.

Mitochondria-targeted complex may be a potential direction bearing on enhancing PDT effects [13]. However, there is still a lack of specific biomarkers and effective therapeutic targets of OSCC. In a recent study, we found a novel malignancy determinant, GBAS that function as a mitochondrion-targeted factor to determine malignant potential in the development of OSCC [14]. When CAL-27 and Tca-8113 cells receiving GBAS short hairpin RNA (shRNA) transfection, the capacities of proliferation, apoptosis, cell cycle and tumorigenesis were significantly regulated and the expression of the proteins related to p53 signalling pathway was notably changed. Additionally, poor outcomes were associated with the high expression of GBAS in all patients with OSCC. As a mitochondrial matrix protein, GBAS is thought to be involved in the process of oxidative phosphorylation and associated with OXPHOS-disorders [15,16]. Norwegian scientists also observed that both GABS and the protein of the same family send a "eat me" mitophagy signal from the surface of the damaged mitochondria. In this study, HeLa cells are unable to clear their damaged mitochondria through mitophagy when there is a depletion of the proteins. Double knockout of both NIPSNAP1 and NIPSNAP2 can inhibit PRKN/Parkin-mediated mitophagy [17]. Furthermore, HeLa cells transfected with siRNA against GBAS can reduce the cellular ATP level [18]. Therefore, the protein plays important roles in cellular energy metabolism.

Gene/drug dual delivery system has developed rapidly in recent years Based on ionic crosslinking and electrostatic adsorption, chitosan (CS) nanocomposite has been widely served as a multifaceted non-viral delivery vector for biomacromolecules and shRNA [19]. To confirm whether the novel mitochondria-targeted gene can enhance the tumor suppression efficacy of ALA-PDT, in this study, we prepared CS nanoparticles (NPs) with the combined co-delivery of ALA photosensitizer and shGBAS plasmid (p)DNA (Fig. 1) to identify anti-cancer effects for OSCC *in vitro* and *in vivo*. In addition, the vector not only displayed robust gene knockdown efficiency in OSCC cells, but also showed low negligible cytotoxicity in normal oral mucosa cells.

2. Material and methods

2.1. Materials

CS (degree of deacetylation, 90 %; $M_w = 50$ kDa) were purchased from Sigma-Aldrich (St. Louis, MO, USA). The pLenti-U6-GFP-P2A-Puro-shGBAS that targeted the GBAS mRNA sequence (TTCGTAAGGCAA-GAAGTGAC) were purchased from Vigene Biosciences (Jinan, China). ALA was a kind gift from Fudan-Zhangjiang Bio-Pharmaceutical Co., Ltd (Shanghai, China). Tripolyphosphatesodium (TPP), acetic acid, Fluorescein isothiocyanate (FITC), and the other chemicals also were obtained from Sigma-Aldrich (St. Louis, MO, USA). Both Dulbecco's modified Eagle's medium (DMEM) and fetal bovine serum (FBS) were sourced from Gibco (Invitrogen, Carlsbad, CA, USA).

2.2. Cell lines and culture

Oral squamous carcinoma cell lines that included WSU-HN6 and CAL-27 cells and oral mucous fibroblasts (OMF) cells were obtained from American Type Culture Collection (ATCC, USA). Human embryonic kidney derived 293 T were purchased from the Cell Resource Center, Shanghai Institute for Biological Sciences, Chinese Academy of Science (Shanghai, China). Both cells were maintained at 37 °C, 5% CO₂ in DMEM containing 10 % FBS. Media were supplemented with 1% antibiotics.

2.3. Synthesis of CS-ALA-shGBAS NPs

CS and CS-ALA NPs were formulated by ionic crosslinking as described in the previous study [20]. Briefly, CS was added to in 1% (v/v) acetic acid, and stirred overnight at room temperature. After filtering to remove the unbound chemicals, CS solution was obtained at concentrations of 3 mg/mL. The NPs were prepared by the dropwise addition of TPP solution (5 mg/mL), and stabilized by CS and TPP in a mass ratio of 6:1. The reaction mixture were then collected by centrifugation (12,000 rpm, 40 min). Under the above conditions, the CS-ALA NPs were also cross-linked by glutaraldehyde (CS:ALA:glutaraldehyde = 7:3:1). Subsequently, the negatively charged shGBAS pDNA and positively charged CS-ALA was mixed through an electrostatic interaction in HEPES buffer medium with a mass ratio of 1:10–1:1, respectively. The mass ratios of CS-ALA and shGBAS pDNA were 1: 10, 1: 5, 1: 2 and 1: 1, respectively. The NPs thus formed were kept at 4 °C.

2.4. Gel retardation assay

The binding of shGBAS pDNA/CS-ALA NPs were analyzed by agarose gel electrophoresis. In brief, samples were prepared by incubating CS-ALA NPs with shGBAS pDNA at a constant voltage of 100 V for 1 h in HEPES buffer (pH 7.4). Complexes were subjected to the agarose gel (The mass ratios of CS-ALA and shGBAS pDNA were 1: 10, 1: 5, 1: 2 and 1: 1), six bands were obtained, including simple use of CS-ALA NPs and pDNA.

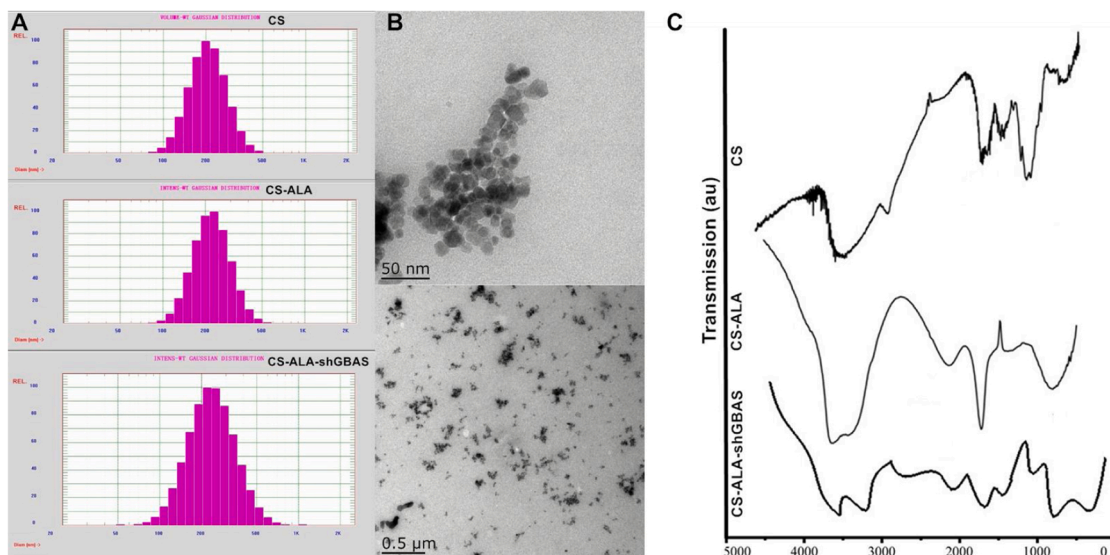


Fig. 2. Physicochemical property of various CS NPs. (A) Particle size distribution histograms of CS, CS-ALA and CS-ALA-shGBAS NPs obtained by DLS data. (B) TEM images of CS-ALA-shGBAS NPs. (C) FT-IR spectra of CS, CS-ALA and CS-ALA-shGBAS NPs.

2.5. Characterization of nanoparticles

Initially, we characterized the particle size, zeta potential and polydispersity index (PDI) of NPs by dynamic light scattering (Nicomp 380 ZLS submicron particle sizer, Preferred Systems Solutions, Inc., Santa Barbara, CA, USA), and the NPs morphology and size were determined by a transmission electron microscope (TEM; FEI Company, Hillsboro, OR, USA) at 25 °C. The methods for characterization were described in detail elsewhere [21].

NPs were lyophilized and the dried samples were compressed into the pelletizings on potassium bromide. Then the structures and composing of prepared samples were analyzed by Fourier transform infrared spectroscopy (FT-IR). The above experiments were done in triplicate.

2.6. Mitochondrial membrane potential detections

We measured the mitochondrial transmembrane potential in WSU-HN6 and CAL-27 cells after treatment with CS-ALA-shGBAS NPs-mediated PDT using JC-1 (5,5',6,6'-tetrachloro-1,1',3,3'-tetraethylbenzimidazolylcarbocyanine iodide) assay kit (Solarbio, Beijing, China). The prepared cells were observed using a fluorescence microscope and detected by flow cytometry. JC-1 can enter into mitochondria and change color reversibly from orange to green as the membrane potential increases. Then, the red-to-green fluorescence intensity ratio was measured. According to the instructions, the decrease in the ratio of red/green fluorescent intensity can indicate mitochondrial depolarization.

2.7. Transcription-polymerase chain reaction (RT-PCR) analysis

Total RNA was isolated from cells by using the TRIzol Reagent (Pufei, Cat. No. 3101-100, Shanghai, China) according to the manufacturer's protocol. Reaction mixture containing total RNA was reverse transcribed to cDNA using M-MLV Reverse Transcriptase (Promega, Cat. No. M1705, Madison, WI, USA). The data was calculated by $2^{-\Delta\Delta Ct}$ method. Two groups of cells were used to compare: control group and CS-ALA-shGBAS group (n = 3).

2.8. PDT experiments

WSU-HN6 and CAL-27 cells were seeded on a 96-well plate at 5×10^3 cells per cm^2 , and incubated *in vitro* with ALA or NPs. After 4 h, cells

were irradiated with a He-Ne ion laser (635 nm, $18 \text{ mW}/\text{cm}^2$, LH-600 Leiye Laser Technology Co., Ltd., Tianjin, China). The light energy densities of laser were $10 \text{ J}/\text{cm}^2$ and $108 \text{ J}/\text{cm}^2$ *in vitro* and *in vivo*, respectively. A power density of $0.2 \text{ W}/\text{cm}^2$ were used *in vitro* and *in vivo*. The proper irradiation time was calculated by the formulation 1 [7].

$$\text{Time(s)} = \frac{\text{Light energy density}(\text{J}/\text{cm}^2)}{\text{Power density}(\text{W}/\text{cm}^2)} \quad (1)$$

2.9. Cytotoxicity and cell viability assays

Cytotoxicity was measured using a 3-[4,5-dimethylthiazol-2-yl]-2,5-diphenyl tetrazolium bromide (MTT) kit (Genview Cat. No. JT343, Beijing, China), according to the following formulation 2.

$$\text{Relative growth rate(RGR)} = \frac{\text{OD}(\text{sample})}{\text{OD}(\text{control})} \times 100\% \quad (2)$$

Briefly, cells were planted into 96-well plates and incubated at 37 °C. After treatment completion in the experimental and control groups, 20 μL MTT solution at a concentration of 5 mg/mL was added to each well and incubated for 4 h. After removing the supernate, 10 μL of dimethyl sulfoxide (DMSO) was added to each well. The absorbance was detected at 490/570 nm using an automatic microplate reader (BioTek, ELX808, USA).

2.10. ROS detections

ROS formation of CS-ALA-shGBAS NPs-mediated PDT was evaluated as the instructions of ROS detection kit. Each NPs solution was mixed with 10 μM 2,7-dichlorofluorescein diacetate (DCFH₂-DA) solution and incubated for 30 min at 37 °C. The cells were detected by a microplate reader (excitation wavelength at 488 nm and emission wavelength at 525 nm).

2.11. Animal experiments

An experimental xenograft model of OSCC was established in athymic nude mice (Vital River Laboratory Animal Technology Co., Ltd, Beijing, China). The animal experiments were approved by the Institutional Animal Care and Use Committee of the Peking University Health Science Center (LA2018-70). All mice received humane care according to the university's ethical guide lines. WSU-HN6 cells were

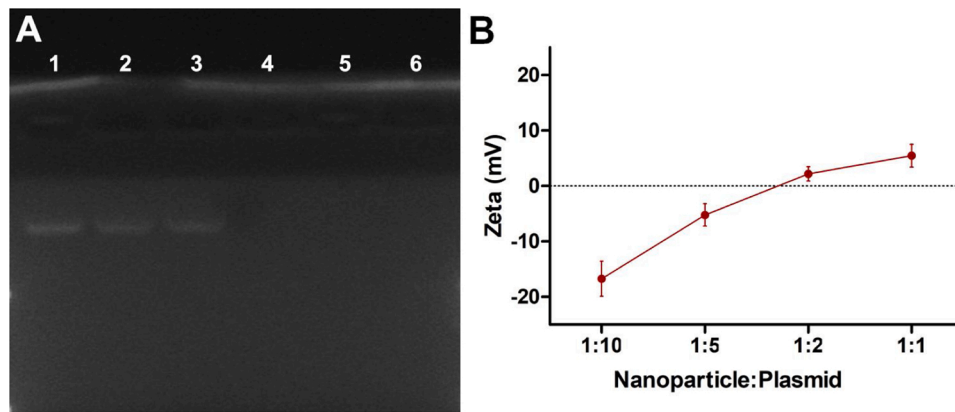


Fig. 3. Complex test of CS-ALA NPs with shGBAS plasmid DNA. (A) Complex formation test using agarose gel electrophoresis. 1: only plasmid DNA, 2-5: weight ratio of NPs/pDNA: 1:10, 1:5, 1:2, 1:1, 6: only NPs (B) Zeta potential assay of CS-ALA-shGBAS NPs with various mass ratios.

subcutaneously inoculated in 50 μL of PBS into the right axilla of six-week old female nude mice under general anesthesia. About two weeks later, the tumor volume reached 100 mm^3 . Mice were randomly divided into four groups ($n = 5$): PBS control group, ALA-NPs-mediated PDT group, shGBAS-NPs group and CS-ALA-shGBAS NPs-mediated PDT group. For local administration, 3 mg/mL ALA, shGBAS or CS-ALA-shGBAS was treated once every week with intratumoral injections in the above experimental group. And 4 h later, mice were irradiated with He-Ne ion laser at 108 J/cm^2 for PDT treatment in the ALA-NPs-mediated PDT and CS-ALA-shGBAS NPs-mediated PDT groups. Gross tumor volume of all nude mice were measured using Vernier caliper (every 3 days). On day 20, the animals were euthanized, and the tumor growth curves were drawn. Gross tumor volume (cm^3) = $3.14/6 \times \text{length} \times \text{width}$ [2].

2.12. Statistical analyses

All data were expressed as the mean \pm standard deviation (SD) of three independent experiments. All statistical analyses were performed using SPSS 17.0 Software (SPSS, Chicago, IL, USA). Statistical differences between two groups were assessed by two-tailed Student's *t*-test, with $p < 0.05$ as the minimal level of significance.

3. Results and discussion

3.1. Preparation and characterization of NPs

Based on our results, the CS-ALA-shGBAS was successfully ionic crosslinked by electrostatic interaction to form a nano-composite structure. The diameters of various NPs were measured by dynamic

light scattering (DLS). The average particle diameter of CS NPs was 209.51 ± 13.17 nm, whereas the diameters of CS-ALA NPs and CS-ALA-shGBAS NPs were 230.20 ± 22.01 and 254.3 ± 9.42 nm, respectively (Fig. 2A). In addition, TEM micrographs showed the morphology of CS-ALA-shGBAS NPs were of approximate homogeneous spherical with a lower PDI of 0.12 ± 0.03 (Fig. 2B).

FT-IR spectra showed the characteristic absorption peak from CS, CS-ALA and CS-ALA-shGBAS NPs, thus validating the success of the above synthesis method. The C=O, C—O and N—H stretching frequencies occur at 1652 and 1099 and 1454 cm^{-1} for CS NPs. Previous data indicated that ALA had unique vibrational features [22,23], The C=O of ALA was observed at 2113 cm^{-1} , while the C=O (1643 cm^{-1}), C—O (825 cm^{-1}) and N—H (1334 cm^{-1}) stretching vibration of CS appeared in the FT-IR spectra of CS-ALA NPs. After the synthesis and mixing of CS, ALA and shGBAS pDNA, the new amide peak absorption of GBAS were also generated. Moreover, vibrational bands representing the above ingredients were all present in CS-ALA-shGBAS NPs (Fig. 2C). In short, the favourable physicochemical properties indicated that our CS-ALA-shGBAS NPs could potentially function as a co-delivery system.

3.2. Agarose gel retardation and zeta potential assay of CS-ALA-shGBAS NPs

CS-ALA-shGBAS complex formation was determined by agarose gel electrophoresis. With the increasement of mass ratios, the electrostatic charge of shGBAS pDNA was neutralized by CS-ALA NPs. As shown in Fig. 3A, the complexes were no longer migrated from the cathode to the anode in gel electrophoresis when mixed at 1: 2 or more in Nanoparticle/Plasmid (N/P) mass ratio, indicating binding between positively charged CS-ALA NPs and negatively charged shGBAS pDNA.

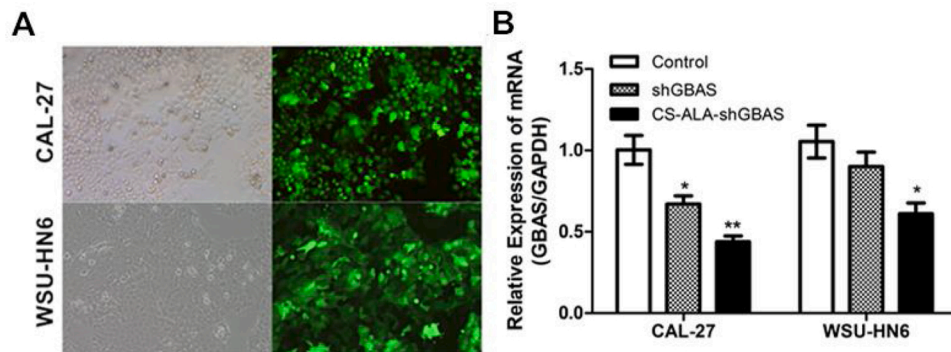


Fig. 4. The morphology of OSCC cells, assessment of transfection efficiency of shGBAS and the expression of GBAS by RT-PCR. (A) Transfection efficiency was detected using fluorescence microscopy at $\times 100$ magnification to observe cells expressing green fluorescent protein. (B) The mRNA expression of GBAS by the RT-PCR in WSU-HN6 and CAL-27 cells (* $p < 0.05$ and ** $p < 0.01$).

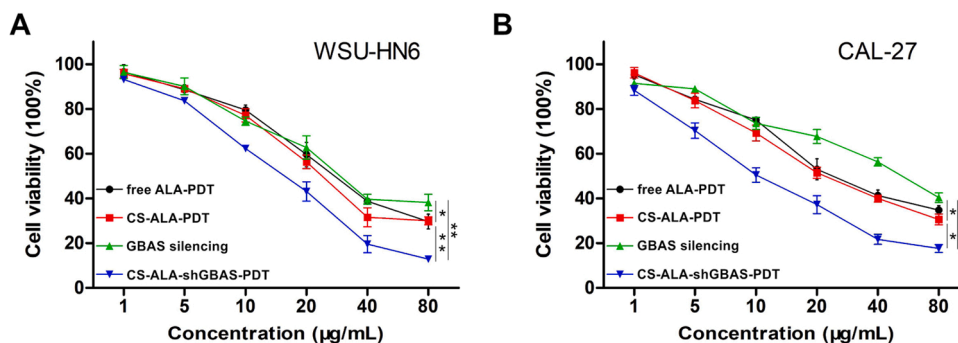


Fig. 5. Cell viability of WSU-HN6 cells (A) and CAL-27 cells (B) treated with various CS NPs (* $p < 0.05$ and ** $p < 0.01$). In all the above experiments, the data were performed independently in triplicate and presented as the mean \pm SD.

The DLS technique was also applied to assess the zeta potential of various NPs. At pH 7.4, the zeta potential was equal to 22.57 ± 0.81 mV for CS NPs and 19.43 ± 0.32 mV for CS-ALA NPs (data not shown). Aside from its use in drug delivery, CS and CS derivatives possess a series of characteristics that show promise as the non-viral gene delivery vector [24]. Since the pDNA is negatively charged, they form complexes with cationic polymers (Fig. 3B). Thus, shGBAS pDNA was adsorbed by electrostatic forces on CS-ALA NPs with cationic nature.

3.3. GBAS gene transfection evaluation

Gene transfection studies by nanocomposites were of great meaning for the new target of gene therapeutic applications. Thus, we evaluated the influence of CS-ALA-shGBAS NPs on gene expression, which were conducted using fluorescence microscopy. After a 72 h transfection, CS-ALA-shGBAS NPs performed superior luciferase activity on OSCC cells (Fig. 4A). Furthermore, the GBAS mRNA expression were measured by RT-PCR analysis, and the expression level were significantly down-regulated in CS-ALA-shGBAS group than that in the control group and single shGBAS group (Fig. 4B). Additionally, the interference effect of NPs on the expression of GBAS gene were differences between WSU-HN6 ($p < 0.05$) and CAL-27 ($p < 0.01$) cells.

3.4. Cytotoxicity study and cell viability assay

Cytotoxicity is the most important indicator for evaluating the safety of non-viral vectors. Thus, we examined the cytotoxicity of CS-ALA-shGBAS NPs at various concentration (5, 25, 50, 100, 250, 500 $\mu\text{g}/\text{mL}$) range in normal oral mucosa fibroblasts cells. The results shown in Fig. S1 demonstrated that CS-ALA-shGBAS NPs showed a consistent and good viability at all concentrations tested. The fundamental reason for hypotoxicity is the application of CS derived from the deacetylation of chitin. Also, the method for synthesizing this co-delivery systems is secure and stable. Furthermore, the biological properties of CS can neutralize the surface charge of plasmids [25].

Next, we determined whether a combination of ALA with shGBAS pDNA would generate a suppressive effect on OSCC *in vitro*. OSCC cell lines were divided into four groups: free ALA-PDT group, GBAS silencing NPs group, ALA-PDT NPs group and combination treatment group based on CS-ALA-shGBAS NPs-mediated PDT. When using the MTT assay for evaluation the combination therapy (80 $\mu\text{g}/\text{mL}$ CS-ALA-shGBAS NPs) showed the greatest inhibition effects in cell proliferation for OSCC cells. The IC₅₀ of CS-ALA-shGBAS NPs-mediated PDT treated WSU-HN6 and CAL-27 cells were 15.43 and 11.15 $\mu\text{g}/\text{mL}$, respectively. The optimum inhibition efficiencies for OSCC cells were both obtained in the combination treatment group at 80 $\mu\text{g}/\text{mL}$ CS-ALA-shGBAS NPs, which the viability of WSU-HN6 and CAL-27 was approximately $12.87 \pm 1.00\%$ and $17.61 \pm 1.82\%$, respectively. Moreover, the combination treatment group exerts more significantly inhibitory effects than either GBAS silencing or ALA-PDT on the growth of OSCC cells (Fig. 5A and B).

Consistent with the previous studies, CS could enhance the antitumor activity of ALA-PDT and gene therapy with good biocompatibility, low immunogenicity [26–28].

3.5. Assay for mitochondrial membrane potential

Mitochondrial membrane potential can reflect the cellular localization of drug action, JC-1 assay was often used for measuring the change of membrane potential and evaluating the functional status in cancer cells [29,30]. Viewing the treated cells under a fluorescent microscope, we were able to identify the degree of membrane potential via cationic fluorescent probe JC-1. The healthy cells displayed higher membrane potential (red fluorescent) as compared to cells intervened by mitochondria-targeting therapy (green fluorescent) [31]. Besides of ALA-PDT, shGBAS could also target mitochondria to trigger ROS (Fig. 6A). [7,14] Compared with PDT and gene silencing alone, PDT using CS-ALA-shGBAS NPs resulted in a significant lower red-to-green fluorescence intensity ratio of WSU-HN6 and CAL-27 cells (Fig. 6B), and results of flow cytometry were statistically analyzed and shown in the bar graph (Fig. 6C). In this study, we showed that this nanocomposite may be a probable mitochondrial targeting anticancer agent. In this study, we showed that this nanocomposite may be a probable mitochondrial targeting anticancer agent.

3.6. Increase in mitochondrial ROS after treatment with CS-ALA-shGBAS NPs-mediated PDT

ROS is an indicator of mitochondrial injury, while a greater increase in ROS generation suggests more cancer cell death induced by oxidative stress [32,33]. In Fig. 7, the remarkable increase in ROS levels was demonstrated when WSU-HN6 and CAL-27 cells were treated by CS-ALA-shGBAS NPs-mediated PDT ($p < 0.01$). Although either ALA-PDT or shGBAS silencing also could lead to ROS generation ($p < 0.05$), ROS levels in them were not statistically different from each other ($p > 0.05$). Similar to mitochondrial membrane potential, the results demonstrated the important role of CS-ALA-shGBAS NPs-mediated PDT in toxic cell killing, which was probably mediated via augmented ROS production.

3.7. CS-ALA-shGBAS NPs suppresses tumour growth in vivo

To further determine whether CS-ALA-shGBAS NPs-mediated PDT could contribute to suppress tumorigenesis in OSCC, a xenograft model with WSU-HN6 cells stably transfected was used in Balb/c nude mice. At 20 d post-grafting, the volumes of xenograft tumour in the combination group were significantly lesser than those of other groups: control group, GBAS-deficient group and ALA-PDT group (Fig. 8A and B). However, Together, these results indicated that the combination group based on CS-ALA-shGBAS NPs effectively reduced the growth of OSCC cells *in vivo*.

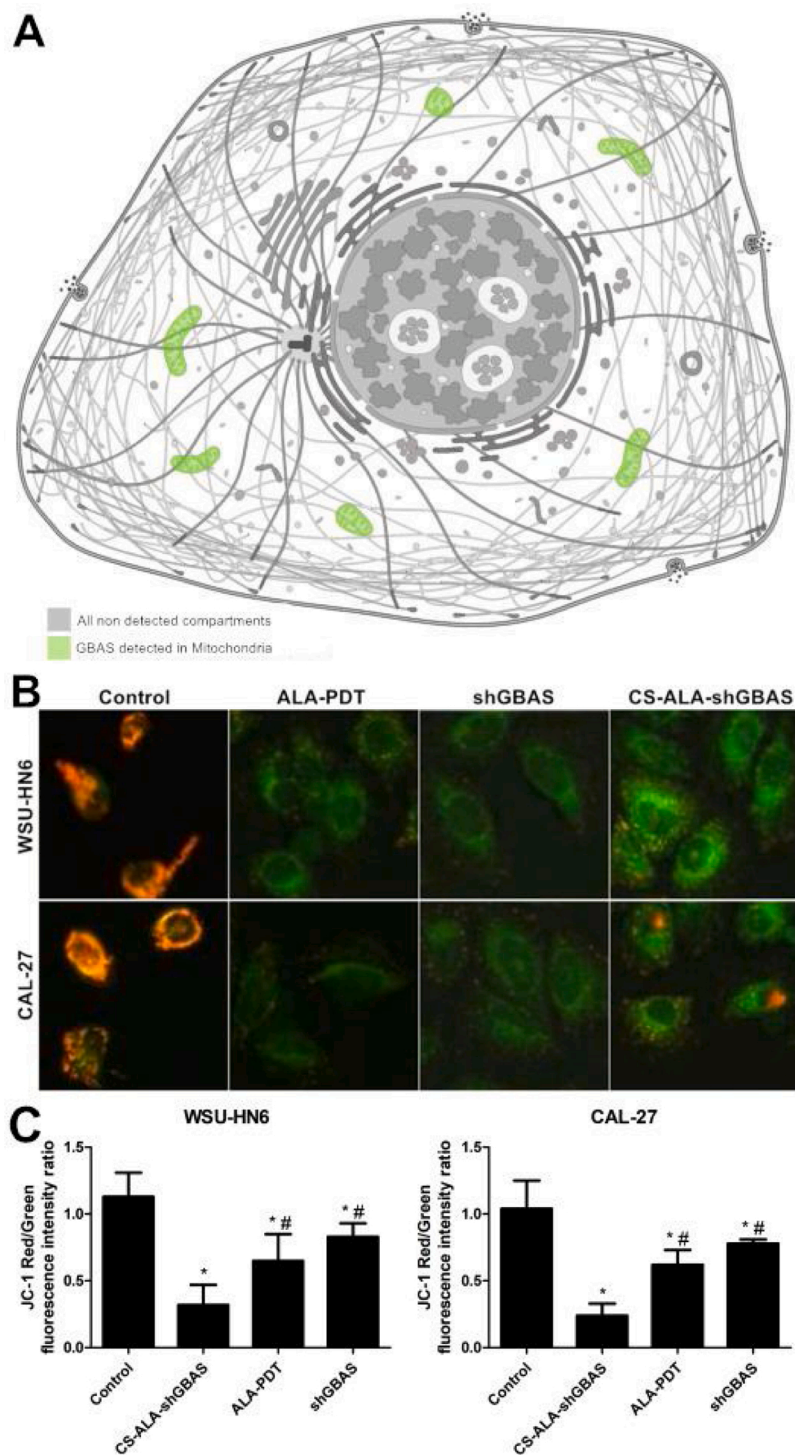


Fig. 6. Cellular uptake and localization of NPs in WSU-HN6 cells and CAL-27 cells. (A) The intracellular distribution of GBAS was validated by the Human Protein Atlas (<http://www.proteinatlas.org/>). (B) JC-1 dye-stained cells were identified the degree of mitochondria membrane potential by a fluorescent microscope. (C) Mitochondrial membrane potential was calculated as the ratio of red/green fluorescence intensity via flow cytometry (* $P < 0.05$ vs. Control group, # $P < 0.05$ vs. CS-ALA-shGBAS group).

4. Conclusions

Mitochondrially targeted nanoparticles have great therapeutic and biotechnological potential for treatment of cancer and other diseases. Emerging research in mitochondria targeted compounds is focused on inducing ROS accumulation and modulating antiproliferative pathways in human cancer cells [34,35]. In general, the delivery of targeted gene to mitochondria is the core of NPs for efficient gene therapy vehicles. Previous studies revealed that GBAS could not only play an important role in supporting cancer growth, but also increasing the susceptibility of mitochondria targeted therapy [14,36]. Good anticancer activity of

shGBAS pDNA was observed through increased intracellular ROS generation and altered mitochondrial membrane potential (Fig. 6B, Fig. 7).

Another line of thought designs a co-delivery system that optimizes traditional therapies use, such as chemotherapy and PDT [37,38]. ALA-PDT has been recognized as a new and minimally invasive treatment for OSCC, because of generating mitochondrial ROS overproduction [39]. We demonstrated that ROS were elevated in both cells. In this study, we found that ROS generation of both cells were elevated in ALA-PDT group (Fig. 7). Moreover, compared with free ALA mediated PDT, treating with PDT based on CS-ALA NPs showed more influence on cell viability. Thus, we assumed that CS NPs increased the

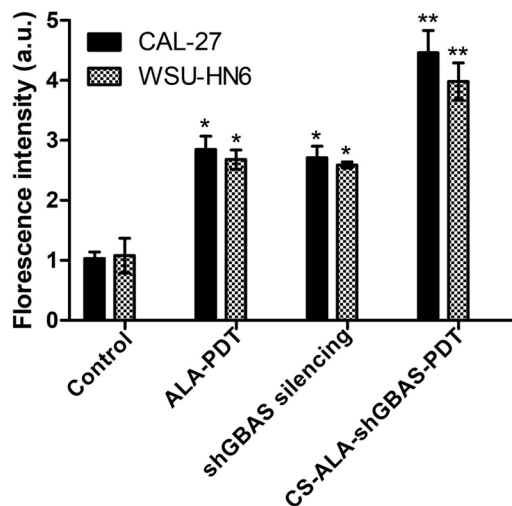


Fig. 7. Cellular ROS after treatment was compared among. ROS levels of WSU-HN6 cells and CAL-27 cells were measured by DCFH-DA fluorescence staining assay kit (* $P < 0.05$ and ** $P < 0.01$).

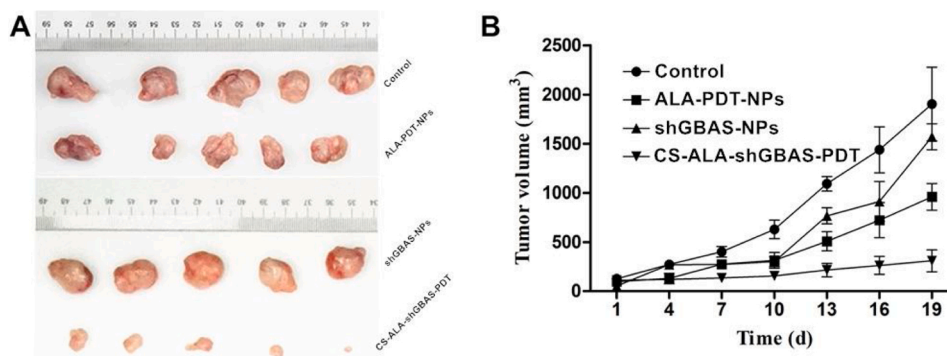


Fig. 8. Tumor growth inhibition in nude mice bearing WSU-HN6 cells following treatment with different formulations. (A) After sacrifice, xenograft tumors *in vivo* and excised tumors were measured. (B) Tumor volume was estimated by different preparations. Data are shown as the mean \pm SD ($n = 5$).

photosensitizer uptake of OSCC cells, and then validated the antitumor action of a novel drug and gene co-delivery system *in vitro* and *in vivo* (Fig. 5A and B, Fig. 8A and B).

In summary, the data of this study revealed a OSCC novel gene/drug dual delivery system for the first time. While the current data are limited and unable to support an in-depth hypothesis, they provide a direction for future research. Future studies on the role of CS-ALA-shGBAS NPs in PDT will facilitate the development of tumour-specific therapeutics targeting mitochondria metabolism.

Funding

This work was supported by National Natural Science Foundation of China (Grant No 81771071) and Jiangsu Province Medical Youth Talent Project (QNRC2016390).

Declaration of Competing Interest

The authors have no conflicts of interest to declare.

Acknowledgments

None.

Appendix A. Supplementary data

Supplementary material related to this article can be found, in the online version, at doi:<https://doi.org/10.1016/j.pdpdt.2021.102218>.

References

- [1] S.A. Koyfman, N. Ismaila, D. Crook, et al., Christopher Holsinger. Management of the neck in squamous cell carcinoma of the oral cavity and oropharynx: ASCO clinical practice guideline, *J. Clin. Oncol.* 37 (20) (2019) 1753–1774.
- [2] S. Zhang, R. Zheng, Q. Chen, et al., Oral cancer incidence and mortality in China, 2011, *Chin. J. Cancer Res.* 27 (1) (2015) 44–51.
- [3] S.B. Chinn, J.N. Myers, Oral cavity carcinoma: current management, controversies, and future directions, *J. Clin. Oncol.* 33 (29) (2015) 3269–3276.
- [4] X. Wang, J. Meng, Efficacy of brachytherapy concomitant with chemotherapy with docetaxel, cisplatin, and 5-fluorouracil in unresectable head and neck squamous cell carcinoma, *J. BUON* 21 (3) (2016) 588–593.
- [5] G. Lodi, R. Franchini, S. Warnakulasuriya, et al., Interventions for treating oral leukoplakia to prevent oral cancer, *Cochrane Database Syst. Rev.* 2016 (7) (2016), CD001829.
- [6] Y. Han, S. Xu, J. Jin, et al., Primary clinical evaluation of photodynamic therapy with oral leukoplakia in chinese patients, *Front. Physiol.* 9 (2018) 1911.
- [7] X. Wang, J. Jin, W. Li, et al., Differential *in vitro* sensitivity of oral precancerous and squamous cell carcinoma cell lines to 5-aminolevulinic acid-mediated photodynamic therapy, *Photodiagnosis Photodyn. Ther.* 29 (2020), 101554.
- [8] R. Saini, N.V. Lee, K.Y. Liu, et al., Prospects in the application of photodynamic therapy in oral cancer and premalignant lesions, *Cancers (Basel)*. 8 (9) (2016) 83.
- [9] S. Mallidi, S. Anbil, A.L. Bulin, et al., Beyond the barriers of light penetration: strategies, perspectives and possibilities for photodynamic therapy, *Theranostics*. 6 (13) (2016) 2458–2487.

- [10] R. Hilf, Mitochondria are targets of photodynamic therapy, *J. Bioenerg. Biomembr.* 39 (1) (2007) 85–89.
- [11] H. Zhao, R. Yin, Y. Wang, et al., Modulating mitochondrial morphology enhances antitumor effect of 5-ALA-mediated photodynamic therapy both *in vitro* and *in vivo*, *J. Photochem. Photobiol. B* 176 (2017) 81–91.
- [12] F.C.P. Rosin, M.G. Teixeira, C. Pelissari, L. Corrêa, Resistance of oral cancer cells to 5-ALA-mediated photodynamic therapy, *J. Cell. Biochem.* 119 (4) (2018) 3554–3562.
- [13] S. Wen, D. Zhu, P. Huang, Targeting cancer cell mitochondria as a therapeutic approach, *Future Med. Chem.* 5 (1) (2013) 53–67.
- [14] X. Wang, Y. Bai, Y. Han, J. Meng, H. Liu, Downregulation of GBAS regulates oral squamous cell carcinoma proliferation and apoptosis via the p53 signaling pathway, *Onco. Ther.* 12 (2019) 3729–3742.
- [15] X.Y. Wang, D.I. Smith, W. Liu, et al., GBAS, a novel gene encoding a protein with tyrosine phosphorylation sites and a transmembrane domain, is co-amplified with EGFR, *Genomics* 49 (3) (1998) 448–451.
- [16] P. Smits, R.J. Rodenburg, J.A. Smeitink, et al., Sequence variants in four candidate genes (NIPSNAP1, GBAS, CHCHD1 and METT11D1) in patients with combined oxidative phosphorylation system deficiencies, *J. Inher. Metab. Dis.* 33 (2010) S13–19.
- [17] Y.P. Abudu, S. Pankiv, B.J. Mathai, et al., NIPSNAP1 and NIPSNAP2 act as "Eat me" signals for mitophagy, *Dev. Cell* 49 (4) (2019) 509–525.
- [18] R.S. Martherus, W. Sluiter, E.D. Timmer, et al., Functional annotation of heart enriched mitochondrial genes GBAS and CHCHD10 through guilt by association, *Biochem. Biophys. Res. Commun.* 402 (2) (2010) 203–208.
- [19] A. Babu, R. Ramesh, Multifaceted applications of chitosan in Cancer drug delivery and therapy, *Mar. Drugs* 15 (4) (2017) 96.
- [20] X. Wang, P. Gao, Y. Yang, et al., Dynamic and programmable morphology and size evolution via a living hierarchical self-assembly strategy, *Nat. Commun.* 9 (1) (2018) 2772.
- [21] Y. Zheng, C. Su, L. Zhao, et al., Chitosan nanoparticle-mediated co-delivery of shAtg-5 and gefitinib synergistically promoted the efficacy of chemotherapeutics through the modulation of autophagy, *J. Nanobiotechnology* 15 (1) (2017) 28.
- [22] A. Filip, S. Clichici, A. Muresan, et al., Effects of PDT with 5-aminolevulinic acid and chitosan on Walker carcinosarcoma, *Exp. Oncol.* 30 (3) (2008) 212–219.
- [23] H. Tahmasebi, K. Khoshgard, A. Sazgarnia, et al., Enhancing the efficiency of 5-aminolevulinic acid-mediated photodynamic therapy using 5-fluorouracil on human melanoma cells, *Photodiagnosis Photodyn. Ther.* 13 (2016) 297–302.
- [24] B. Santos-Carballeda, E. Fernández Fernández, F.M. Goycoolea, Chitosan in non-viral gene delivery: role of structure, characterization methods, and insights in cancer and rare diseases therapies, *Polymers (Basel)*. 10 (4) (2018) 444.
- [25] M.D. Buschmann, A. Merzouki, M. Lavertu, et al., Chitosans for delivery of nucleic acids, *Adv. Drug Deliv. Rev.* 65 (9) (2013) 1234–1270.
- [26] C. Thunshelle, R. Yin, Q. Chen, et al., Current advances in 5-Aminolevulinic acid mediated photodynamic therapy, *Curr. Dermatol. Rep.* 5 (3) (2016) 179–190.
- [27] T.L. Cupino, B.A. Watson, A.C. Cupino, et al., Stability and bioactivity of chitosan as a transfection agent in primary human cell cultures: a case for chitosan-only controls, *Carbohydr. Polym.* 180 (2018) 376–384.
- [28] I. Postiglione, A. Chiavieello, G. Palumbo, et al., Enhancing photodynamic therapy efficacy by combination therapy: dated, current and oncoming strategies, *Cancers (Basel)*. 3 (2) (2011) 2597–2629.
- [29] A. Perelman, C. Wachtel, M. Cohen, et al., JC-1: alternative excitation wavelengths facilitate mitochondrial membrane potential cytometry, *Cell Death Dis.* 3 (11) (2012) e430.
- [30] S.T. Smiley, M. Reers, C. Mottola-Hartshorn, et al., Intracellular heterogeneity in mitochondrial membrane potentials revealed by a J-aggregate-forming lipophilic cation JC-1, *Proc. Natl. Acad. Sci. U. S. A.* 88 (9) (1991) 3671–3675.
- [31] K. Elefantova, B. Lakatos, J. Kubickova, et al., Detection of the mitochondrial membrane potential by the cationic dye JC-1 in L1210 cells with massive overexpression of the plasma membrane ABCB1 drug transporter, *Int. J. Mol. Sci.* 19 (7) (2018) 1985.
- [32] S. Pustynnikov, F. Costabile, S. Beghi, et al., Targeting mitochondria in cancer: current concepts and immunotherapy approaches, *Transl. Res.* 202 (2018) 35–51.
- [33] M. Vara-Perez, B. Felipe-Abrio, P. Agostinis, Mitophagy in cancer: a tale of adaptation, *Cells*. 8 (5) (2019) 493.
- [34] A.K. Camara, E.J. Lesnfsky, D.F. Stowe, Potential therapeutic benefits of strategies directed to mitochondria, *Antioxid. Redox Signal.* 13 (3) (2010) 279–347.
- [35] J. Zielonka, J. Joseph, A. Sikora, et al., Mitochondria-targeted triphenylphosphonium-based compounds: syntheses, mechanisms of action, and therapeutic and diagnostic applications, *Chem. Rev.* 117 (15) (2017) 10043–10120.
- [36] R.S. Martherus, W. Sluiter, E.D. Timmer, et al., Functional annotation of heart enriched mitochondrial genes GBAS and CHCHD10 through guilt by association, *Biochem. Biophys. Res. Commun.* 402 (2010) 203–208.
- [37] M.D. Glasgow, M.B. Chougule, Recent developments in active tumor targeted multifunctional nanoparticles for combination chemotherapy in cancer treatment and imaging, *J. Biomed. Nanotechnol.* 11 (11) (2015) 1859–1898.
- [38] B. Xiao, L. Ma, D. Merlin, Nanoparticle-mediated co-delivery of chemotherapeutic agent and siRNA for combination cancer therapy, *Expert Opin. Drug Deliv.* 14 (1) (2017) 65–73.
- [39] S. Iinuma, S.S. Farshi, B. Ortel, et al., A mechanistic study of cellular photodestruction with 5-aminolevulinic acid-induced porphyrin, *Br. J. Cancer* 70 (1) (1994) 21–28.